# Structural Basis of Transcription Activation: The CAP-αCTD-DNA Complex

Brian Benoff,[1] Huanwang Yang,[1] Catherine L. Lawson,[1] Gary Parkinson,[1]* Jinsong Liu,[1]† Erich Blatter,[1,2]‡ Yon W. Ebright,[1,2] Helen M. Berman,[1]§ Richard H. Ebright[1,2]‖

The *Escherichia coli* catabolite activator protein (CAP) activates transcription at $P_{lac}$, $P_{gal}$, and other promoters through interactions with the RNA polymerase α subunit carboxyl-terminal domain (αCTD). We determined the crystal structure of the CAP-αCTD-DNA complex at a resolution of 3.1 angstroms. CAP makes direct protein-protein interactions with αCTD, and αCTD makes direct protein-DNA interactions with the DNA segment adjacent to the DNA site for CAP. There are no large-scale conformational changes in CAP and αCTD, and the interface between CAP and αCTD is small. These findings are consistent with the proposal that activation involves a simple "recruitment" mechanism.

The catabolite activator protein (CAP) [also referred to as the cyclic adenosine monophosphate (cAMP) receptor protein] activates transcription by binding to a DNA site located in or upstream of the core promoter and interacting with the RNA polymerase (RNAP) α subunit COOH-terminal domain (αCTD) [reviewed in (*1*)], an 85–amino acid, independently folded domain that is flexibly tethered to the remainder of RNAP [reviewed in (*2*)]. Interaction of CAP with αCTD facilitates binding of αCTD (and, through it, the remainder of RNAP) to promoter DNA, thereby stimulating transcription initiation (*1*). At class I CAP-dependent promoters, such as the $P_{lac}$ promoter, CAP-αCTD interaction is the sole basis of activation (*1*). At class II CAP-dependent promoters, such as the $P_{gal}$ promoter, interaction of CAP with αCTD is one of multiple interactions involved in activation (*1, 3*).

CAP binds to DNA as a dimer of two identical subunits and recognizes a 22–base pair (bp), two-fold symmetric consensus DNA site (*1, 4–6*). Transcription activation by CAP requires a determinant within CAP termed "activating region 1" (AR1) (residues 156 to 164) (*1, 7–11*), which is functionally presented by one of the two subunits of the CAP dimer (*1, 12, 13*). Transcription activation also requires the COOH-terminal residue of CAP (residue 209) (*14*), which, in the structure of the CAP-DNA complex, is located adjacent to, and is in contact with, AR1 (*6*).

Transcription activation by CAP requires three distinct determinants within αCTD (*1, 15–19*): (i) the "287 determinant" (residues 285 to 290, 315, 317, and 318), proposed to mediate protein-protein interaction with AR1 of CAP; (ii) the "265 determinant" (residues 265, 294, 296, 298, 299, and 302), proposed to mediate protein-DNA interaction with the DNA segment adjacent to the DNA site for CAP; and (iii) the "261 determinant" (residues 257, 258, 259, and 261), proposed to mediate protein-protein interaction with $\sigma^{70}$ at a subset of class I CAP-dependent promoters, including $P_{lac}$.

Transcription activation by CAP also requires the structural integrity of the DNA segment adjacent to the DNA site for CAP (*1, 20*). In the ternary complex of CAP, RNAP, and promoter, αCTD interacts with the DNA segment adjacent to the DNA site for CAP, contacting the DNA minor groove centered 18 or 19 bp from the center of the DNA site for CAP (*1, 21, 22*). At most CAP-dependent promoters, including $P_{lac}$, αCTD interacts nonspecifically with the DNA segment adjacent to the DNA site for CAP, contacting arbitrary, nonspecific DNA sequences (*1, 23, 24*). However, replacement of these nonspecific DNA sequences by high-affinity, specific DNA sites for αCTD (e.g., 5′-AAAAAA-3′) (*25*) facilitates formation of the ternary complex of CAP, RNAP, and promoter (*1, 24, 26–28*).

In previous work, the CAP-DNA complex was crystallized using a 30-bp two-fold symmetric DNA fragment containing the 22-bp two-fold symmetric consensus DNA site for CAP and 4 bp of flanking DNA on each side (Fig. 1A, top) [(*6*); see also (*4, 5*)]. In our current work, we crystallized the CAP-αCTD-DNA complex using an analogous 44-bp two-fold symmetric DNA fragment containing the 22-bp two-fold symmetric consensus DNA site for CAP and 11 bp of flanking DNA—with an optimally positioned, high-affinity, specific DNA site for αCTD (i.e., 5′-AAAAAA-3′) (*25, 27, 28*)—on each side (Fig. 1B, top) (*29*). It was anticipated that this DNA fragment would yield a two-fold symmetric complex consisting of a central CAP dimer flanked on each side by αCTD (Fig. 1B).

The structure was solved by molecular replacement using the crystal structure of the CAP-DNA complex as the initial model and iterative cycles of Fourier refinement and model building to place the rest of the structure. The final model $R$ and $R_{free}$ values are, respectively, 21.1 and 24.4% against 3.1 Å diffraction data (Fig. 1C) (*30*).

As anticipated, the two-fold symmetric crystallization DNA fragment yielded a two-fold symmetric structure (Fig. 1B). Each half of the two-fold symmetric structure contains one subunit of CAP, one-half of the crystallization DNA fragment, one molecule of αCTD that interacts with CAP and DNA ($\alpha CTD^{CAP,DNA}$), and one molecule of αCTD that interacts exclusively with DNA, interacting with an A/T-rich DNA-minor-groove segment that, fortuitously, is accessible in the crystal lattice ($\alpha CTD^{DNA}$). We suggest that the structure defines two distinct sets of biologically relevant interactions: (i) CAP-αCTD-DNA interactions at a class I or class II CAP-dependent promoter (Fig. 2; CAP-$\alpha CTD^{CAP,DNA}$-DNA) and (ii) αCTD-DNA interactions with an A/T-rich DNA minor groove at an UP element subsite–dependent promoter [Fig. 3; $\alpha CTD^{DNA}$-DNA (*2, 25*)].

The structures of the CAP-DNA complex (Fig. 1A) (*6*) and of CAP-DNA within the present complex (Fig. 1B) are superimposable [root mean square deviation of backbone atoms ($RMSD_{backbone}$) = 1.0 Å]. We conclude that the conformations of CAP and the DNA segment in contact with CAP do not change substantially upon interaction with αCTD. Similarly, the structures of free αCTD (*31*), $\alpha CTD^{CAP,DNA}$, and $\alpha CTD^{DNA}$ are superimposable ($RMSD_{backbone}$ = 0.7 to 2.1 Å). We conclude that the conformation of αCTD does not change substantially upon interaction with CAP and/or with DNA. The structure of the DNA segment between CAP and $\alpha CTD^{CAP,DNA}$ is moderately distorted (roll of 15° and twist deficit of 10° centered 13 bp from the center of the DNA site for CAP, resulting in compression by ~2.5 Å of the DNA major groove centered 13 bp from the center of the DNA site for CAP, and reduction by ~7.5 Å of the distance between CAP and $\alpha CTD^{CAP,DNA}$) (*32, 33*). The struc-

[1]Waksman Institute and Department of Chemistry, [2]Howard Hughes Medical Institute, Rutgers University, Piscataway, NJ 08854, USA.
*Present address: CRC Biomolecular Structure Unit, Institute of Cancer Research, London SW3 6JB, UK.
†Present address: Tularik Inc., South San Francisco, CA 94080, USA.
‡Present address: Human Genome Sciences Inc., Rockville, MD 20874, USA.
§To whom correspondence on crystallographic issues should be addressed. E-mail: berman@rutchem.rutgers.edu
‖To whom correspondence on all other issues should be addressed. E-mail: ebright@mbcl.rutgers.edu

tures of the DNA segments in contact with $\alpha CTD^{CAP,DNA}$ and $\alpha CTD^{DNA}$ are nearly canonical B-form DNA, with only very slight distortion (compression by ~1.5 Å of the DNA minor groove).

The interaction between CAP and $\alpha CTD^{CAP,DNA}$ involves AR1 and the COOH-terminal residue of CAP and the 287 determinant of $\alpha CTD^{CAP,DNA}$ (Fig. 2, A through C). The interaction involves a strikingly small interface (six residues each of CAP and αCTD; 630 $Å^2$ of buried surface area). Residues 157 to 160 and 164 of AR1 contact residues 285 to 288 of the 287 determinant, with the $Thr^{158}$ side-chain hydroxyl making two hydrogen bonds (to residues 285 and 286), the $Thr^{158}$ backbone carbonyl making two hydrogen bonds (to residues 285 and 287), the $Thr^{158}$ side-chain methyl making van der Waals interactions (to residue 286), and residues 157, 159, 160, and 164 making additional van der Waals interactions (Fig. 2B). The COOH-terminal residue of CAP ($Arg^{209}$) contacts residues 315 and 317 of the 287 determinant of αCTD, with the COOH-terminal residue side chain making a hydrogen bond to residue 315 and the COOH-terminal backbone carboxylate making a salt bridge with residue 317 (Fig. 2C). The COOH-terminal residue side chain also makes two buttressing hydrogen bonds to AR1 (to backbone carbonyl oxygens of residues 159 and 160). The observed contacts provide a structural rationalization for genetic results indicating that $Thr^{158}$ is the critical residue in AR1 (the only residue in AR1 for which side-chain atoms beyond Cβ are required for activation) (*10*) and indicating involvement of residues 157 to 160, 164, and the COOH-terminus of CAP, and residues 285 to 288, 315, and 317 of αCTD (*1, 7–11, 14, 18, 19*). The structure also provides a rationalization for genetic results indicating involvement of residues 162 and 163 of CAP and residues 289 and 290 of αCTD (*1, 8–11, 19*); in the structure, these residues underlie (and make hydrogen bonds and van der Waals interactions with) residues of AR1 and the 287 determinant of αCTD and, as such, are likely to be critical determinants of the conformations of AR1 and the 287 determinant. The observed small size of the interface between CAP and $\alpha CTD^{CAP,DNA}$ is in agreement with genetic results ruling out involvement of other residues (*10, 18, 19*) and with biochemical results indicating a modest magnitude of transcriptional activation (a factor of about 10 at $P_{lac}$) (*34*) and a modest magnitude of CAP-RNAP interaction free energy (about –1 to –2 kcal/mol at $P_{lac}$) (*35–37*).

The interaction between $\alpha CTD^{CAP,DNA}$ and DNA involves the 265 determinant of $\alpha CTD^{CAP,DNA}$ and the DNA backbone and minor groove of the 6-bp DNA segment centered 19 bp from the center of the DNA site for CAP (5′-AAAAAG-3′) (Fig. 2, A, D, and E). Residues 264, 265, 268, 294, 296, 298, and 299 of the 265 determinant make direct contacts with the DNA backbone (Fig. 2, D and E). No residue makes direct contacts with DNA base-pair edges (Fig. 2, D and E). However, the $Arg^{265}$ side chain penetrates into the DNA minor groove and makes at least two, and possibly four, water-mediated hydrogen bonds with DNA base-pair edges (cyan in Fig. 2, D and E). The $Arg^{265}$ side-chain guanidinium makes two water-mediated hydrogen bonds (to the thymine O2 atom of the A:T base pair 18.5 bp from the center of the DNA site for CAP, and to the adenine N3 atom of the A:T base pair 19.5 bp from the center of the DNA site for CAP) through interaction with a water molecule positioned as in the "minor-groove spine of water" characteristic of A/T-rich DNA (*38–41*) (cyan in Fig. 2, D and E). In addition, the $Arg^{265}$ side-chain guanidinium is positioned so as potentially to make two additional water-mediated hydrogen bonds (to the thymine O2 atom of the A:T base pair 19.5 bp from the center of the DNA site for CAP, and to the adenine N3 atom of the A:T base pair 20.5 bp from the center of the DNA site for CAP) through interaction with a putative second water molecule positioned as in the minor-groove spine of water (a water molecule not

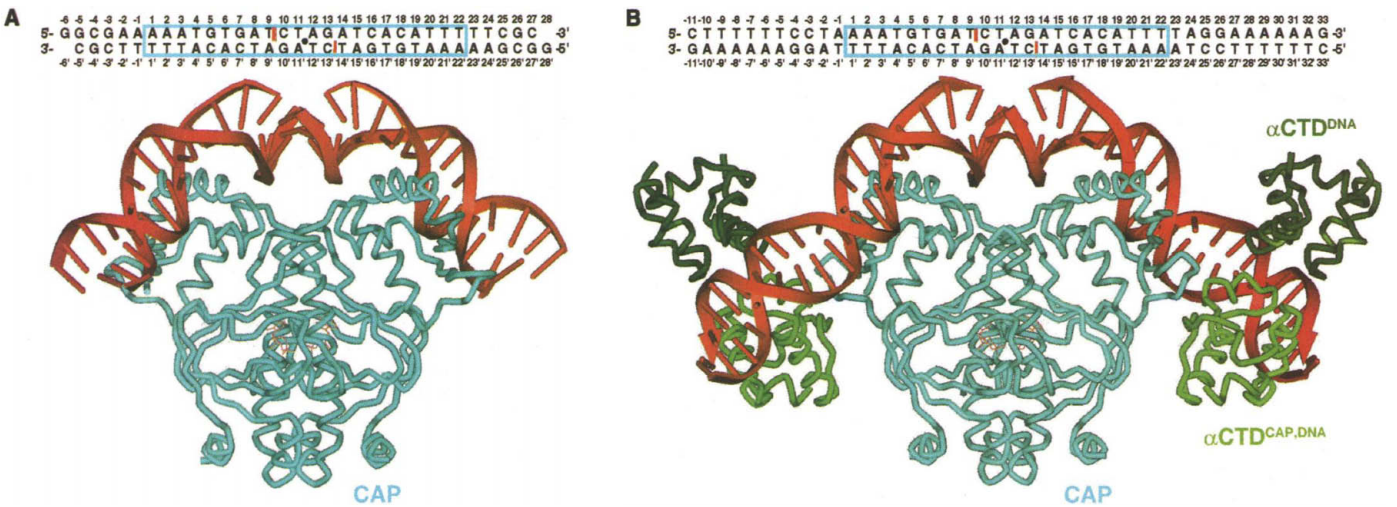


**Fig. 1.** Structure determination. (**A**) Top, 30-bp DNA fragment used to crystallize the CAP-DNA complex in (*6*) (box, DNA site for CAP; solid circle, two-fold symmetry axis of DNA site for CAP; solid bars, single-phosphate gaps). Bottom, structure of the CAP-DNA complex in (*6*). CAP is in cyan; DNA and cAMP are in red. (**B**) Top, 44-bp DNA fragment used to crystallize the CAP-αCTD-DNA complex in this work (box, DNA site for CAP; solid circle, two-fold symmetry axis of DNA site for CAP; solid bars, single-phosphate gaps). Bottom, structure of the CAP-αCTD-DNA complex of this work. CAP is in cyan, $\alpha CTD^{CAP,DNA}$ is in light green, $\alpha CTD^{DNA}$ is in dark green, and DNA and cAMP are in red. (**C**) Crystallographic data collection and refinement statistics. *I*, intensity.

**C**

| | Native | Brominated |
|---|---|---|
| Wavelength (λ) | 1.100 | 1.100 |
| Temperature (°K) | 100 | 100 |
| Space Group | $P6_222$ | $P6_222$ |
| Unit Cell (Å) | a=b=175.97 c=158.02 α=β=90° γ=120° | |
| Resolution (Å) | 20.0-3.1 | 50-3.5 |
| Measured Reflections | 332,877 | 357,426 |
| Unique Reflections | 23,331 | 18,915 |
| Mosaicity | 0.29 | 0.60 |
| Completeness (%) | 88.0 | 95.0 |
| I/σ(I) | 13.7 | 13.9 |
| R-merge | 7.6 | 8.5 |
| R-cryst (%) | 21.1 | |
| R-free (%) | 24.4 | |

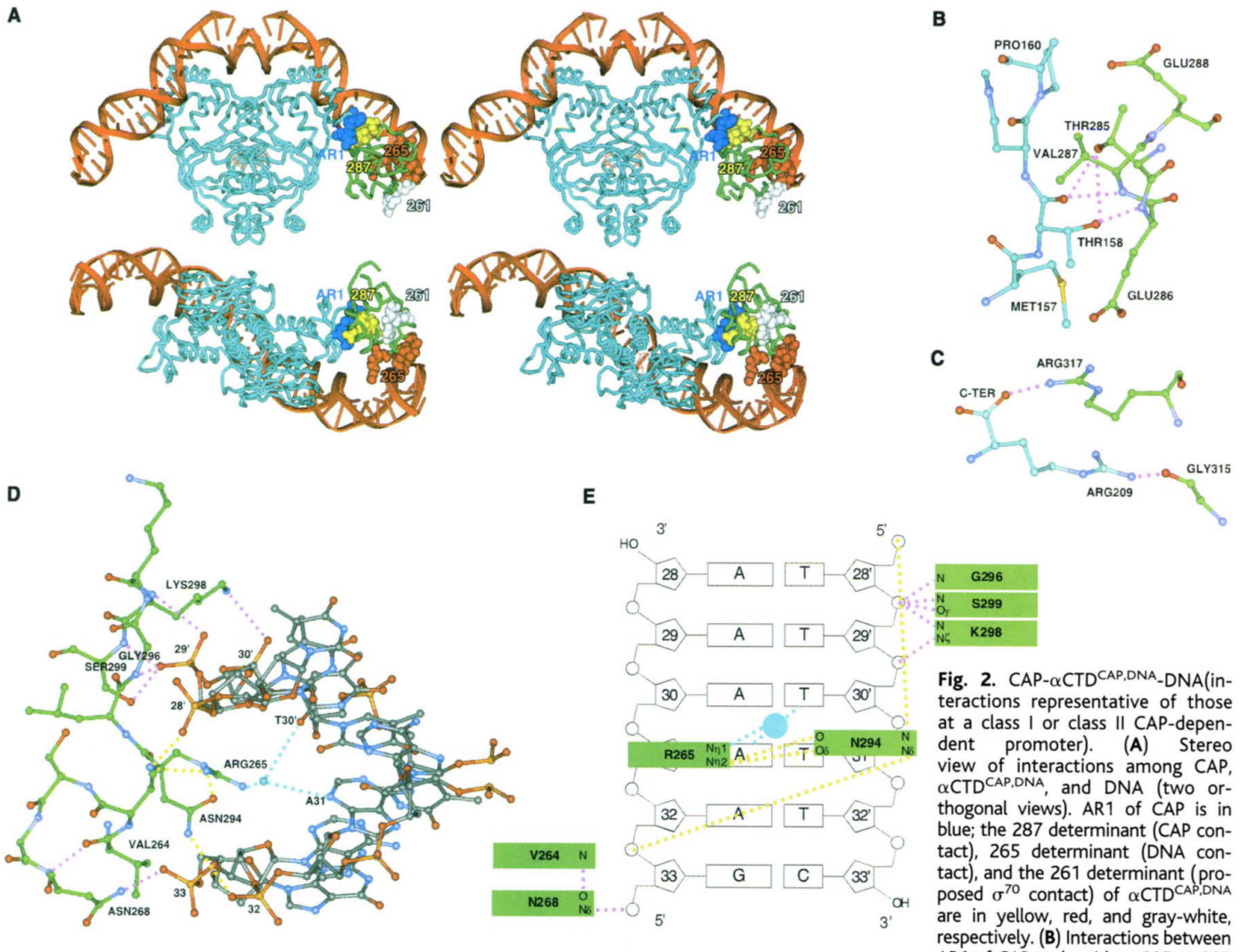


**Fig. 2.** CAP-αCTD$^{CAP,DNA}$-DNA(interactions representative of those at a class I or class II CAP-dependent promoter). **(A)** Stereo view of interactions among CAP, αCTD$^{CAP,DNA}$, and DNA (two orthogonal views). AR1 of CAP is in blue; the 287 determinant (CAP contact), 265 determinant (DNA contact), and the 261 determinant (proposed $\sigma^{70}$ contact) of αCTD$^{CAP,DNA}$ are in yellow, red, and gray-white, respectively. **(B)** Interactions between AR1 of CAP and residues 285 to 288 of the 287 determinant of αCTD$^{CAP,DNA}$. Hydrogen bonds are in magenta. **(C)** Interactions between the COOH-terminal residue of CAP (Arg$^{209}$) and residues 315 and 317 of the 287 determinant of αCTD$^{CAP,DNA}$. Hydrogen bonds are in magenta. C-TER, COOH-terminus. **(D)** Interactions between αCTD$^{CAP,DNA}$ and DNA (view along DNA minor-groove axis). Water-mediated hydrogen bonds involving the Arg$^{265}$ side-chain guanidinium, DNA bases, and an experimentally defined water molecule (sphere near center) are in cyan. The network of hydrogen bonds buttressing the Arg$^{265}$ side-chain guanidinium relative to the phosphate backbones of the two DNA strands is in yellow. Other hydrogen bonds are in magenta. **(E)** Summary of interactions between αCTD$^{CAP,DNA}$ and DNA. Colors are as in (D). G, Gly; K, Lys; N, Asn; R, Arg; S, Ser; and V, Val.

observed in this structure at 3.1 Å) (*39*). The Arg$^{265}$ side-chain guanidinium is held in a precise orientation relative to the DNA minor groove and bound water through buttressing van der Waals interactions with DNA-backbone sugars of the top and bottom DNA strands (Fig. 2D) and by a cross-helix network of buttressing hydrogen bonds, involving two hydrogen bonds between the Arg$^{265}$ side-chain guanidinium and Asn$^{294}$, one hydrogen bond between Asn$^{294}$ and a DNA-backbone phosphate of the top DNA strand, and one hydrogen bond between Asn$^{294}$ and a DNA-backbone phosphate of the bottom DNA strand (yellow in Fig. 2, D and E). The observed contacts provide a structural rationalization for genetic and nuclear magnetic resonance (NMR)–spectroscopic results indicating involvement of residues 264, 265, 268, 294, 296, 298, and 299 (with Arg$^{265}$ as the most critical residue) in CAP-αCTD-DNA and αCTD-DNA interactions (*1, 15–19, 25, 42, 43*), for biochemical and NMR-spectroscopic results indicating involvement of the DNA minor groove in CAP-αCTD-DNA and αCTD-DNA interactions (*22, 43, 44*), and for interference-footprinting results indicating involvement of the adenine N3 atom in αCTD-DNA interactions (*44*). The observed contacts also provide two structural rationalizations for the specificity of αCTD for A/T-rich DNA: (i) Arg$^{265}$ makes water-mediated hydrogen bonds through interaction with the minor-groove spine of water, a structural feature present in A/T-rich DNA (*40, 41*), and (ii) Arg$^{265}$ is buttressed by a network of interactions spanning a compressed, narrowed minor groove, a structural feature present in A/T-rich DNA (*45, 46*).

The 261 determinant of αCTD$^{CAP,DNA}$ is located on the face of αCTD$^{CAP,DNA}$ opposite from CAP, ~23 bp from the center of the DNA site for CAP, and is prominently exposed (gray-white in Fig. 2A). The position and prominent exposure of the 261 determinant are consistent with the proposal that the 261 determinant participates in αCTD-$\sigma^{70}$ interactions at the subset of class I CAP-dependent promoters, including $P_{lac}$, where CAP binds in the −60 region, with ~23 bp between the center of the DNA site for CAP and the upstream edge of the DNA segment contacted by $\sigma^{70}$ (*1, 19, 47*).

As noted above, the crystal structure contains a second molecule of αCTD that interacts exclusively with DNA, interacting with an UP element subsite–like DNA segment (5′-GAAAAA-3′) [compare with (*25*)] that, fortuitously, is accessible in the crystal lattice: αCTD$^{DNA}$ (dark green in Fig. 1B; Fig.

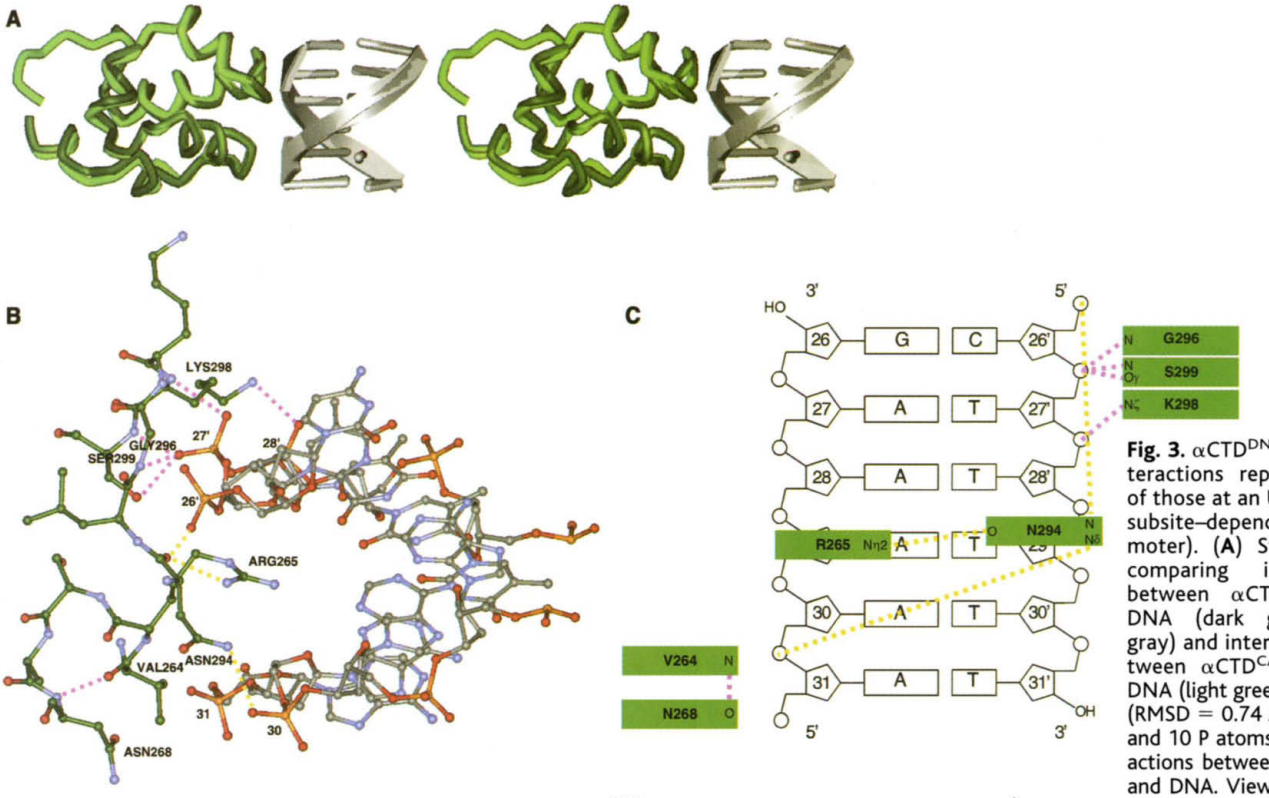


**Fig. 3.** $\alpha CTD^{DNA}$-DNA (interactions representative of those at an UP element subsite–dependent promoter). (**A**) Stereo view comparing interactions between $\alpha CTD^{DNA}$ and DNA (dark green and gray) and interactions between $\alpha CTD^{CAP\text{-}DNA}$ and DNA (light green and gray) (RMSD = 0.74 Å for 72 Cα and 10 P atoms). (**B**) Interactions between $\alpha CTD^{DNA}$ and DNA. View and colors are as in Fig. 2D. No water molecules were observed in the $\alpha CTD^{DNA}$-DNA interface in this structure at 3.1 Å. However, the positions of the $Arg^{265}$ side-chain guanidinium and DNA bases are compatible with the establishment of water-mediated hydrogen bonds identical to those at the $\alpha CTD^{CAP,DNA}$-DNA interface (Fig. 2D) (*39*). (**C**) Summary of interactions between $\alpha CTD^{DNA}$ and DNA. Colors are as in Fig. 2, D and E.

3). $\alpha CTD^{DNA}$-DNA and $\alpha CTD^{CAP,DNA}$-DNA interactions are nearly identical, both in overall organization and in detail (Fig. 3). We infer that similar αCTD-DNA interactions are made in UP element subsite–dependent transcription and in CAP-dependent transcription, consistent with similar requirements for the 265 determinant (*1, 15–19, 25, 42, 43*) and similar preferences for A/T-rich DNA (*24–28*).

The results in this report provide a high-resolution structural description of interactions between a transcriptional activator and its target within the general transcription machinery. Two striking findings are that transcriptional activation can occur without conformational change in activator and target and that transcriptional activation can involve a small interface between activator and target. These findings support the proposal that transcriptional activation can involve a simple "recruitment" mechanism—that is, simple "adhesive" interactions between activator and target that facilitate and/or stabilize interaction of the general transcription machinery with promoter DNA (*1, 2, 48–50*). Activation by recruitment does not require conformational signaling within or through the target; does not require extensive, high-information-content interactions between activator and target; and entails modest net interaction energies between activator and target (interaction energies comparable to the magnitude of activation) (*48–50*). We suggest that the results provide a structural paradigm for understanding other examples of transcriptional activation, both in bacteria (where most activators are thought to function through recruitment and to contact the same target, αCTD) (*1, 2, 48–50*) and in eukaryotes (where most activators are thought to function through recruitment) (*49, 50*).

### References and Notes


1. S. Busby, R. Ebright, *J. Mol. Biol.* **293**, 199 (1999).
2. ———, *Cell* **79**, 743 (1994).
3. W. Niu, Y. Kim, G. Tau, T. Heyduk, R. Ebright, *Cell* **87**, 1123 (1996).
4. S. Schultz, G. Shields, T. Steitz, *Science* **253**, 1001 (1991).
5. G. Parkinson *et al.*, *J. Mol. Biol.* **260**, 395 (1996).
6. G. Parkinson *et al.*, *Nature Struct. Biol.* **3**, 837 (1996).
7. A. Bell *et al.*, *Nucleic Acids Res.* **18**, 7243 (1990).
8. A. Eschenlauer, W. Reznikoff, *J. Bacteriol.* **173**, 5024 (1991).
9. Y. Zhou, X. Zhang, R. Ebright, *Proc. Natl. Acad. Sci. U.S.A.* **90**, 6081 (1993).
10. W. Niu, Y. Zhou, Q. Dong, Y. Ebright, R. Ebright, *J. Mol. Biol.* **243**, 595 (1994).
11. Y. Zhou, T. Merkel, R. Ebright, *J. Mol. Biol.* **243**, 603 (1994).
12. Y. Zhou, S. Busby, R. Ebright, *Cell* **73**, 375 (1993).
13. Y. Zhou *et al.*, *EMBO J.* **13**, 4549 (1994).
14. Z.-H. Yang, J. Krakow, *FASEB J.* **5**, A814 (1991).
15. C. Zou, N. Fujita, K. Igarashi, A. Ishihama, *Mol. Microbiol.* **6**, 2599 (1992).
16. H. Tang *et al.*, *Genes Dev.* **8**, 3058 (1994).
17. K. Murakami, N. Fujita, A. Ishihama, *EMBO J.* **15**, 4358 (1996).
18. N. Savery *et al.*, *EMBO J.* **17**, 3439 (1998).
19. N. Savery *et al.*, *J. Bacteriol.* **184**, 2273 (2002).
20. S. Ryu, S. Garges, S. Adhya, *Proc. Natl. Acad. Sci. U.S.A.* **91**, 8582 (1994).
21. A. Kolb *et al.*, *Nucleic Acids Res.* **21**, 319 (1993).
22. N. Naryshkin, A. Revyakin, Y. Kim, V. Mekler, R. Ebright, *Cell* **101**, 601 (2000).
23. U. Flatow, G. Rajendrakumar, S. Garges, *J. Bacteriol.* **178**, 2436 (1996).
24. D. Czarniecki, R. Noel, W. Reznikoff, *J. Bacteriol.* **179**, 423 (1997).
25. R. Gourse, W. Ross, T. Gaal, *Mol. Microbiol.* **37**, 687 (2000).
26. R. Noel, W. Reznikoff, *J. Mol. Biol.* **282**, 495 (1998).
27. N. Savery, V. Rhodius, H. Wing, S. Busby, *Biochem. J.* **309**, 77 (1995).
28. E. Law, N. Savery, S. Busby, *Biochem. J.* **337**, 415 (1999).
29. Crystals were grown by vapor diffusion at 20°C as hanging drops in solutions containing 0.1 to 0.2 mM CAP (*5*), 0.2 to 0.4 mM αCTD (α residues 245 to 329) (*42*), 0.1 to 0.3 mM DNA fragment [prepared as in (*5*)], and 0.8 mM cAMP in buffer A [50 mM sodium acetate (pH 4.5), 250 mM NaCl], equilibrated against a reservoir containing 2× buffer A. Crystals were stabilized by successive transfers (2 min per transfer) to 2× buffer A containing 5, 10, 15, 20, 25, and 30% ethylene glycol and were mounted on loops and flash frozen at −165°C. Crystals were hexagonal and had space-group symmetry $P6_222$, $a = b = 176$ Å, $c = 158$ Å, $\alpha = \beta = 90°$, $\gamma = 120°$.
30. Data were collected at the X25 beamline [National Synchrotron Light Source (NSLS), Brookhaven National Laboratory] and processed with DENZO and SCALEPACK (*51*). Initial phasing was derived by molecular replacement with AMORE (*52*) using the structure of the CAP-DNA complex at a resolution of 2.2 Å [Protein Data Bank (PDB) accession number 2CGP; residues 9 to 205 of the CAP protomer and nucleotide pairs 13 to 25 of DNA; initial $R = 47.1\%$]. Additional DNA was modeled into electron density in $F_{obs} - F_{calc}$ maps, and analysis of difference-Fourier

electron density from diffraction data collected on a 5-bromouracil derivative (5-bromouracil at positions 11, 23, and 32') was used to confirm the placement of DNA. Helical segments of the solution structure of αCTD (PDB accession number 1COO) were modeled into electron density in $F_{obs} - F_{calc}$ maps, additional residues of CAP and αCTD were modeled into electron density in successive cycles of Fourier refinement, and the structure was refined by using CNS (*53*) with anisotropic initial *B*-factor refinement and bulk solvent correction, incorporating water molecules conservatively, following strict criteria as described (*5*). The completeness of the highest resolution shell (3.2 to 3.1 Å) was 0.4; reflections from the highest resolution shell were included in the refinement. Omit maps, combined with simulated annealing, were used to confirm the placement and conformation of each residue in the structure. The asymmetric unit contains one CAP protomer and two αCTD protomers (2688 nonhydrogen atoms), one DNA half-site (895 nonhydrogen atoms), and 32 water molecules (Fig. 1, B and C). Atomic coordinates have been deposited in the PDB (accession number 1LB2).

31. Y. H. Jeon *et al.*, *Science* **270**, 1495 (1995).
32. DNA helical parameters were analyzed with 3DNA (*54*).
33. The DNA bend between CAP and $\alpha CTD^{CAP,DNA}$ (15° roll, 13 bp from the center of the DNA site for CAP in each half-complex) is not in phase with the DNA bend induced by CAP (44° roll, 5 bp from the center of the DNA site for CAP, and –9° roll, 10 bp from the center of the DNA site for CAP, in each half-complex). Therefore, the overall DNA bend angle in the present complex is similar to that in the CAP-DNA complex (45° versus 46° in each half-complex for PDB accession number 1RUN) (*6*), but the out-of-plane component of DNA bending in the present complex is greater (–39° versus –21° in each half-complex for PDB accession number 1RUN) (*6*).
34. T. P. Malan, A. Kolb, H. Buc, W. McClure, *J. Mol. Biol.* **180**, 881 (1984).
35. D. Straney, S. Straney, D. Crothers, *J. Mol. Biol.* **206**, 41 (1989).
36. Y. L. Ren, S. Garges, S. Adhya, J. Krakow, *Proc. Natl. Acad. Sci. U.S.A.* **85**, 4138 (1988).
37. S. Wang, Y. Shi, I. Gorshkova, F. Schwarz, *J. Biol. Chem.* **275**, 33457 (2000).
38. The presence of the experimental water molecule (cyan in Fig. 2, D and E) is unequivocal (largest peak in $F_{obs} - F_{calc}$ difference map at 4σ; clear in a simulated annealing omit map at 4σ and clear in $2F_{obs} - F_{calc}$ map at 1σ; *B* factor = 36.5).
39. Expected positions of first-shell minor-groove-spine water molecules were calculated as described (*55*). The position of the experimental water molecule (cyan in Fig. 2, D and E) corresponds to the expected position of a first-shell minor-groove-spine water molecule. Expected positions of second-shell minor-groove-spine water molecules were calculated analogously (*56*). The position of the $Arg^{265}$ NH1 atom corresponds to the expected position of a second-shell minor-groove-spine water molecule.
40. M. Kopka, A. Fratini, H. Drew, R. Dickerson, *J. Mol. Biol.* **163**, 129 (1983).
41. H. Berman, B. Schneider, in *Oxford Handbook of Nucleic Acid Structure*, S. Neidel, Ed. (Oxford Univ. Press, Oxford, UK, 1999), pp. 295–312.
42. T. Gaal *et al.*, *Genes Dev.* **10**, 16 (1996).
43. K. Yasuno *et al.*, *J. Mol. Biol.* **306**, 213 (2001).
44. W. Ross, A. Ernst, R. Gourse, *Genes Dev.* **15**, 491 (2001).
45. M. Katahira, H. Sugeta, Y. Kyogoku, *Nucleic Acids Res.* **18**, 613 (1990).
46. D. MacDonald, K. Herbert, X. Zhang, T. Pologruto, P. Lu, *J. Mol. Biol.* **306**, 1081 (2001).
47. H. Chen, R. H. Ebright, unpublished data.
48. S. Dove, J. Joung, A. Hochschild, *Nature* **386**, 627 (1997).
49. M. Ptashne, A. Gann, *Nature* **386**, 569 (1997).
50. _____, *Genes & Signals* (Cold Spring Harbor Laboratory Press, Plainview, NY, 2002).
51. Z. Otwinowski, W. Minor, *Methods Enzymol.* **276**, 307 (1997).
52. J. Navaza, *Acta Crystallogr. A* **50**, 157 (1994).
53. A. Brünger *et al.*, *Acta Crystallogr. D* **54**, 905 (1998).
54. X.-J. Lu, Z. Shakked, W. Olson, *J. Mol. Biol.* **300**, 819 (2000).
55. B. Schneider *et al.*, *Biophys. J.* **65**, 2291 (1993).
56. B. Schneider, H. Berman, unpublished data.
57. We thank A. Napoli and M. Becker for assistance with data collection at NSLS beamline X25 and B. Schneider for discussion. Supported by NIH grants GM21589 (H.B.), GM41376 (R.H.E.), and GM64375 (Ronald Levy and R.H.E.) and by a Howard Hughes Medical Investigatorship (R.H.E.).

**Supporting Online Material**
www.sciencemag.org/cgi/content/full/297/5586/1562/DC1
Figs. S1 and S2

19 July 2002; accepted 29 July 2002

# Identification of a Potential Ejaculation Generator in the Spinal Cord

**William A. Truitt and Lique M. Coolen***

**We tested the significance of a population of lumbar spinothalamic cells for male sexual behavior in rats. These cells are positioned to relay ejaculation-related signals from reproductive organs to the brain, and they express neurokinin-1 receptors. Ablation of these neurons by the selective toxin SSP-saporin resulted in a complete disruption of ejaculatory behavior. In contrast, other components of sexual behavior remained intact. These results suggest that this population of spinothalamic cells plays a pivotal role in generation of ejaculatory behavior and may be part of a spinal ejaculation generator.**

Male sexual behavior is a complex behavior dependent on intrinsic and extrinsic factors, including olfactory, somatosensory, and visceral cues (*1*). The pathways that relay somatosensory and visceral sensory information from the reproductive organs to the brain are not well understood. Recent studies have used expression of the protein product Fos of the immediate early gene c-*fos* to map neural activation in the brain related to the expression of ejaculation in male rodents (*2*). Ejaculation-related Fos induction is restricted to a few brain regions, including areas within the medial amygdala, the bed nucleus of the stria terminalis, and a medial portion of the parvocellular subparafascicular nucleus (SPFp) within the posterior thalamus (*3*). The thalamus receives direct sensory inputs from the spinal cord and may thus be an important relay for genital sensory inputs to other areas of the brain important for sexual behavior. Indeed, the SPFp receives unique inputs from a population of spinothalamic neurons located in laminae VII and X in lumbar segments 3 and 4 (L3 and L4) containing galanin, cholecystokinin (*4–6*), and enkephalin (*7*). Here we refer to this population of lumbar SPFp-projecting neurons as LSt (lumbar spinothalamic) cells. These cells are specifically activated with ejaculation but not with other components of male sexual behavior (*5*, *6*). Thus we hypothesized that LSt neurons are involved in the relay of ejaculation-specific information, although the behavioral significance of these neurons is unknown.

To test the behavioral significance of LSt neurons, effects of lesions of the LSt population on sexual behavior were investigated. LSt neurons are sparsely distributed lateral to the central canal in lamina X and in the medial portion of lamina VII of L3 and L4 and are difficult to lesion by traditional methods. We thus identified a membrane target located on the LSt neurons. It was demonstrated that 93.0 ± 1.7% of LSt neurons express neurokinin-1 receptor (NK-1R) and conversely 84.7 ± 2.47% of NK-1R–containing cells in the area surrounding the central canal at L3 and L4 express galanin (Fig. 1). We therefore used the targeted toxin SSP-saporin (SAP), which consists of the toxin SAP conjugated to SSP, a substance P analog with high affinity for NK-1R (*8*). SSP-SAP was infused into the L3 and L4 spinal cord at the location of the LSt cells in sexually experienced or sexually naïve male rats (*9*). Control animals were injected with unconjugated equimolar concentrations of SAP. The doses used selectively ablate NK-1R–containing cells in vivo without producing nonselective lesions (*8*). Sexual behavior was first tested 10 days after lesion surgery, and during five subsequent twice-weekly tests.

After the final behavior test, animals were perfused, and spinal cord tissue was immunoprocessed for galanin, NK-1R, or neuronal marker N (NeuN) (*9*). Labeled cells were counted in a standard area surrounding the central canal of L3 and L4 sections representative of the location of LSt cells (Fig. 2A, area 1).

Of the 19 rats included in the behavioral

Department of Cell Biology, Neurobiology, and Anatomy; Neuroscience Graduate Program; University of Cincinnati, College of Medicine, Post Office Box 670521, Cincinnati, OH 45267-0521, USA.

*To whom correspondence should be addressed. E-mail: Lique.Coolen@uc.edu